

Strong coupling between phonon-polaritons and plasmonic nanorods

CHRISTIAN HUCK,¹ JOCHEN VOGT,¹ TOMÁŠ NEUMAN,² TADAAKI NAGAO,³ RAINER HILLENBRAND,^{4,5} JAVIER AIZPURUA,² ANNEMARIE PUCCI,¹ AND FRANK NEUBRECH^{1,6,*}

¹Kirchhoff Institute for Physics, Heidelberg University, Im Neuenheimer Feld 227, 69120 Heidelberg, Germany

²Materials Physics Center (CSIC-UPV/EHU) and Donostia International Physics Center (DIPC), Paseo Manuel de Lardizabal 5, 20018 Donostia-San Sebastián, Spain

³WPI Center for Materials NanoArchitectonics (MANA), National Institute for Materials Science, 1-1 Namiki, Tsukuba 305-0044, Japan

⁴CIC nanoGUNE and UPV/EHU, 20018 Donostia-San Sebastián, Spain

⁵IKERBASQUE, Basque Foundation for Science, 48011 Bilbao, Spain

⁶4th Physics Institute, University of Stuttgart, Pfaffenwaldring 57, 70569 Stuttgart, Germany

*f.neubrech@pi4.uni-stuttgart.de

Abstract: We perform far-field spectroscopy of infrared metal antennas on silicon oxide layers of different thickness, where we find a splitting of the plasmonic resonance. This splitting can result in a transparency window, corresponding to suppression of antenna scattering, respectively “cloaking” of the antenna. Backed up by theory, we show that this effect is caused by strong coupling between the metal antenna plasmons and the surface phonon polaritons in the oxide layer. The effect is a kind of induced transparency in which the strength of the phonon-polariton field plays the crucial role. It represents a further tuning possibility for the optical performance of infrared devices.

© 2016 Optical Society of America

OCIS codes: (300.6340) Spectroscopy, infrared; (240.5420) Polaritons; (240.6680) Surface plasmons; (250.5403) Plasmonics.

References and links

1. M.G. Cottam and D.R. Tilley, *Introduction to Surface and Superlattice Excitations* (Cambridge University, 1989).
2. D. Mirlin, “Surface Phonon Polaritons in Dielectrics and Semiconductors,” in *Surface Polaritons Electromagnetic Waves at Surfaces and Interfaces* (Elsevier, 1982).
3. K. L. Kliewer and R. Fuchs, “Optical modes of vibration in an ionic crystal slab including retardation. I. nonradiative region,” *Phys. Rev.* **144**(2), 495–503 (1966).
4. K. L. Kliewer and R. Fuchs, “Optical modes of vibration in an ionic crystal slab including retardation. II. radiative region,” *Phys. Rev.* **150**(2), 573–588 (1966).
5. J. D. Caldwell, L. Lucas, G. Vincenzo, V. Igor, T. L. Reinecke, S. A. Maier, and O. J. Glembocki, “Low-loss, infrared and terahertz nanophotonics using surface phonon polaritons,” *Nanophotonics* **4**(1), 44–68 (2015).
6. T. Wang, P. Li, B. Hauer, D. N. Chigrin, and T. Taubner, “Optical properties of single infrared resonant circular microcavities for surface phonon polaritons,” *Nano Lett.* **13**(11), 5051–5055 (2013).
7. R. Marty, A. Mlayah, A. Arbouet, C. Girard, and S. Tripathy, “Plasphonics: local hybridization of plasmons and phonons,” *Opt. Express* **21**(4), 4551–4559 (2013).
8. N. Ocelic, R. Hillenbrand, A. Arbouet, C. Girard, and S. Tripathy, “Subwavelength-scale tailoring of surface phonon polaritons by focused ion-beam implantation,” *Nat. Mater.* **3**(9), 606–609 (2004).
9. M. S. Anderson, “Enhanced infrared absorption with dielectric nanoparticles,” *Appl. Phys. Lett.* **83**(14), 2964–2966 (2003).
10. H. C. Kim and X. Cheng, “Surface phonon polaritons on sic substrate for surface-enhanced infrared absorption spectroscopy,” *J. Opt. Soc. Am. B* **27**(11), 2393–2397 (2010).
11. P. Törmä and W. L. Barnes, “Strong coupling between surface plasmon polaritons and emitters: a review,” *Rep. Prog. Phys.* **78**(1), 013901 (2015).
12. P. Weis, J. L. Garcia-Pomar, R. Beigang, and M. Rahm, “Hybridization induced transparency in composites of metamaterials and atomic media,” *Opt. Express* **19**(23), 23573–23580 (2011).
13. D. Shelton, I. Brener, J. C. Ginn, M. B. Sinclair, D. W. Peters, K. R. Coffey, and G. D. Boreman, “Strong coupling between nanoscale metamaterials and phonons,” *Nano Lett.* **11**(5), 2104–2108 (2011).

14. J. M. Hoffmann, H. Janssen, D. N. Chigrin, and T. Taubner, "Enhanced infrared spectroscopy using small-gap antennas prepared with two-step evaporation nanosphere lithography," *Opt. Express* **22**(12), 14425–14432 (2014).
15. D. Berreman, "Infrared absorption at longitudinal optic frequency in cubic crystal films," *Phys. Rev.* **130**(6), 2193–2198 (1963).
16. F. Neubrech, D. Weber, D. Enders, T. Nagao, and A. Pucci, "Antenna sensing of surface phonon polaritons," *J. Phys. Chem. C* **114**(16), 7299–7301 (2010).
17. F. Neubrech and A. Pucci, "Plasmonic enhancement of vibrational excitations in the infrared," *IEEE J. Sel. Topics Quantum Electron.* **19**(3), 4600809 (2013).
18. R. Adato and H. Altug, "In-situ ultra-sensitive infrared absorption spectroscopy of biomolecule interactions in real time with plasmonic nanoantennas," *Nat. Commun.* **4**, 2154 (2013).
19. Z. Fei, G. O. Andreev, W. Bao, L. M. Zhang, A. S. McLeod, C. Wang, M. K. Stewart, Z. Zhao, G. Dominguez, M. Thieme, M. M. Fogler, M. J. Tauber, A. H. Castro-Neto, C. N. Lau, F. Keilmann, and D. N. Basov, "Infrared nanoscopy of Dirac plasmons at the graphene-SiO₂ interface," *Nano Lett.* **11**(11), 4701–4705 (2011).
20. I. J. Luxmoore, C. H. Gan, P. Q. Liu, F. Valmorra, P. Li, J. Faist, and G. R. Nash, "Strong coupling in the far-infrared between graphene plasmons and the surface optical phonons of silicon dioxide," *ACS Photonics* **1**(11), 1151–1155 (2014).
21. H. Yan, T. Low, W. Zhu, Y. Wu, M. Freitag, X. Li, F. Guinea, P. Avouris, and F. Xia, "Damping pathways of mid-infrared plasmons in graphene nanostructures," *Nature Photon.* **7**(5), 394–399 (2013).
22. T. Neuman, C. Huck, J. Vogt, F. Neubrech, R. Hillenbrand, J. Aizpurua, and A. Pucci, "Importance of plasmonic scattering for an optimal enhancement of vibrational absorption in SEIRA with linear metallic antennas," *J. Phys. Chem. C* **119**(47), 26652–26662 (2015).
23. M. K. Gunde, "Vibrational modes in amorphous silicon dioxide," *PHYSICA B* **292**(3–4), 286–295 (2000).
24. H. Lüth, *Solid Surfaces, Interfaces and Thin Films* (Springer, 2010).
25. P. Palik, *Handbook of Optical Constants of Solids* (Academic Press, 1985).
26. Y. Jia, H. Zhao, Q. Guo, X. Wang, H. Wang, and F. Xia, "Tunable plasmon-phonon polaritons in layered graphene-hexagonal boron nitride heterostructures," *ACS Photonics* **2**(7), 907–912 (2015).
27. H. Yan, T. Low, F. Guinea, F. Xia, and P. Avouris, "Tunable phonon-induced transparency in bilayer graphene nanoribbons," *Nano Lett.* **14**(8), 4581–4586 (2014).
28. P. Senet, P. Lambin, and A. Lucas, "Standing-wave optical phonons confined in ultrathin overlayers of ionic materials," *Phys. Rev. Lett.* **74**(4), 570–573 (1995).
29. W. Gao, Y. Fujikawa, K. Saiki, and A. Koma, "Surface phonons of LiBr/Si(100) epitaxial layers by high resolution electron energy loss spectroscopy," *Solid State Commun.* **87**(11), 1013–1015 (1993).
30. C. Huck, F. Neubrech, J. Vogt, A. Toma, D. Gerbert, J. Katzmann, T. Härtling, and A. Pucci, "Surface-enhanced infrared spectroscopy using nanometer-sized gaps," *ACS Nano* **8**(5), 4908–4914 (2014).
31. S. Bagheri, K. Weber, T. Gissibl, T. Weiss, F. Neubrech, and H. Giessen, "Fabrication of square-centimeter plasmonic nanoantenna arrays by femtosecond direct laser writing lithography: Effects of collective excitations on SEIRA enhancement," *ACS Photonics* **2**(6), 779–786 (2015).
32. D. Weber, P. Albella, P. Alonso-González, F. Neubrech, H. Gui, T. Nagao, R. Hillenbrand, J. Aizpurua, and A. Pucci, "Longitudinal and transverse coupling in infrared gold nanoantenna arrays: long range versus short range interaction regimes," *Opt. Express* **19**(16), 15047–15061 (2011).
33. D. Dregely, F. Neubrech, H. Duan, R. Vogelgesang, and H. Giessen, "Vibrational near-field mapping of planar and buried three-dimensional plasmonic nanostructures," *Nat. Commun.* **4**, 2237 (2013).
34. L. Novotny, "Effective wavelength scaling for optical antennas," *Phys. Rev. Lett.* **98**(26), 266802 (2007).
35. F. Neubrech, S. Beck, T. Glaser, M. Hentschel, H. Giessen, and A. Pucci, "Spatial extend of plasmonic enhancement of vibrational signals in the infrared," *ACS Nano* **8**(6), 6250–6258 (2014).

1. Introduction

Similar to surface plasmon-polaritons, surface phonon-polaritons (SPhP) are mixed excitations that couple via their dipole moments with electromagnetic radiation [1, 2]. Even though phonon-polaritons have been extensively studied in the literature [3, 4] during the 20th century, the development of technology that allows for reliable fabrication of micron-sized plasmonic nanostructures has led scientists to focus their attention to phenomena occurring when plasmon and phonon polaritons interact [5, 6]. Thus their description is vital for understanding of fundamental phenomena such as opening of transparency windows [7] in the plasmonic spectra and applications like near-field optical microscopy [8] or chemical sensing with surface-enhanced infrared spectroscopy [9, 10]. Especially the strong coupling of two oscillators leading to the formation of a transparency window has attracted great interest [11]. It has been theoretically and experimentally shown by placing metal nanostructures (nanoantennas) on top of thin ionic films that such a strong coupling can occur in the THz and infrared (IR) spectral range [7, 12, 13].

Shelton et al. [13], for example, demonstrated the strong coupling of plasmon polaritons and phonons of a 10 nm thick silicon oxide layer in the IR. In their investigations, the authors only used a single oscillator at the transverse optical frequency and did not consider the polariton dispersion. Also in other studies [14], there is still a lack of knowledge on the nature of the SPhP thin film modes leading to induced transparency, e.g. their near-field distribution or vibrational frequency, which we will discuss in the present paper.

According to the Berreman effect [15], phononic excitations of such a thin ionic layer near the longitudinal optical (LO) phonon frequency cannot be excited in normal transmittance, but at oblique incidence of *p*-polarized light. Interestingly, the LO resonance is also observed when plasmonic antennas are placed on top of the phononic surface [16, 17]. As it has already been reported for a thin film of about 3 nm of natural silicon oxide [16], a Fano-type signal near the LO frequency appears on the background of the plasmonic extinction, even if the plasmonic resonance is detuned away from this frequency. This is in contrast to the simple idea of an enhanced absorption of the oxide layer, since then the vibrational signal should appear near the TO frequency, or, for weakly infrared active oscillators, at the vibrational frequency of the molecule [18].

Recently, such coupling was also observed in the absorption spectrum of graphene nanoribbons caused by the interaction between phonon modes of relatively thick SiO₂ layers (approx. 300 nm) and the plasmonic excitations [19–21]. The important difference to the graphene ribbons is that the gold nanoantennas in this study scatter light with much larger efficiency than the graphene nanoribbons so that in the final extinction spectrum there is a considerable contribution of resonant light scattering involved [22].

In the present study, we will detail the coupling of plasmonic modes to phonon-polariton excitations of nm thick silicon oxide layers leading to the emergence of transparency windows in the plasmonic spectra. Using experimental far-field spectroscopic measurements and the numerical method of finite-difference in time-domain (FDTD) with support of analytical models for the polariton dispersion, we systematically analyze the plasmon phonon-polariton coupling for different configurations of nanometer-thick silicon oxide layers, that mechanically support and optically cloak the metal nanoantennas. It will be shown that, at optimal resonance tuning, the resonant plasmonic extinction decreases with increasing layer thickness up to the opening of a transparency window.

2. Phonon polaritons of planar layers

In the first section, we briefly review the characteristics of the phonon-polariton modes supported by thin oxide layers. Throughout the paper, we will focus our theoretical calculations on a simplified model of SiO₂ phonons that will be represented by a single Lorentz oscillator dielectric function [Fig. 1(a)]. The oscillator describes the real system of the Si–O–Si stretching vibration, as the strongest oscillator with the TO phonon frequency $\omega_{\text{TO}} = 1064 \text{ cm}^{-1}$ (given in photon wavenumbers) in glassy silicon dioxide [23]. For the Lorentzian model used here, the frequency dependent dielectric function is $\varepsilon_{\text{Lorentz}}(\omega) = \varepsilon_{\infty} + \Omega^2/(\omega_{\text{TO}}^2 - \omega^2 - i\gamma\omega)$ where the dielectric background $\varepsilon_{\infty} = 2.14$ and the oscillator strength $\Omega = 950 \text{ cm}^{-1}$ correspond to data of the real oxide [22]. For the spectral and near-field simulations we assume an only weak phonon damping of $\gamma = 10 \text{ cm}^{-1}$. In the calculation of dispersion relations for phonon polaritons this weak damping is neglected, which does not modify conclusions on the assignment of polariton modes. The maximum of the imaginary part of the negative inverse dielectric function, $\Im(-1/\varepsilon_{\text{Lorentz}})$, the so-called energy-loss function, defines the spectral peak position, ω_{LO} , of the LO phonon in the bulk material.

With the dielectric function in hand, we describe the phonon polariton modes of two typical systems that interact with plasmonic antennas. We start with a planar layered structure consisting of semi-infinite silicon substrate (with $\varepsilon_{\text{Si}} = 11.7$) covered by a thin film of the silicon dioxide in

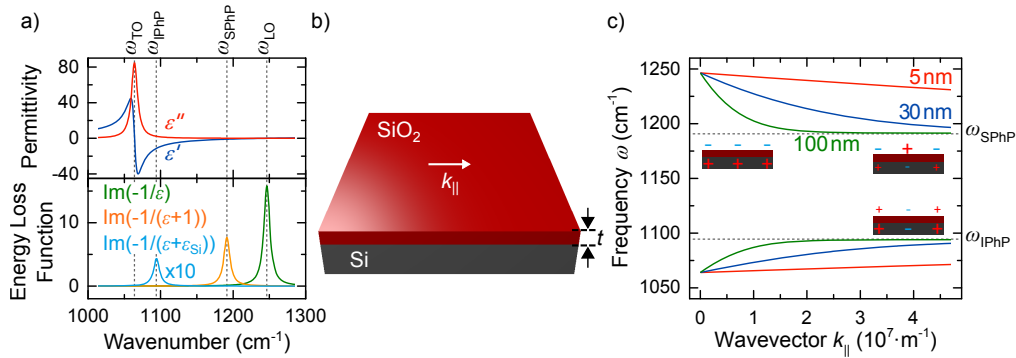


Fig. 1. (a) Dielectric function and derived energy-loss functions of the phononic layer material (similar to SiO₂ in the Si–O stretching range). (b) Sketch of the system under investigation. (c) Quasi static dispersion relations for planar SiO₂ layer with different thickness t , as indicated, on top of the Si substrate and with air superstrate. The horizontal dashed lines mark the SPhP and IPHP frequency ω_{SPhP} and ω_{IPhP} of the SiO₂ to air and of the interface to silicon, respectively. The wavevector k_{\parallel} is parallel to the interface. Insets schematically depict the surface charge distributions characteristic for the surface modes that belong to the respective parts of dispersion relations.

vacuum (or air) environment. Dispersion relations for different layer thickness t are calculated in the quasi-static limit using the one-oscillator dielectric function from above with $\gamma = 0$ [Fig. 1(c)]. For a given thickness t , the dispersion relation consists of a pair of branches. The energetically higher one starts for low k vectors at the frequency of LO phonons (maximum of $\Im(-1/\varepsilon_{\text{Lorentz}})$), and, in the short wavelength limit, asymptotically approaches the frequency of the surface phonon-polariton of a single air-silica interface (ω_{SPhP}) at 1191 cm^{-1} given by the maximum of $\Im(-1/(\varepsilon_{\text{Lorentz}} + 1))$ [24]. Please note that for the real experimental permittivity, the SPhP frequency of the single interface is located below the result from the simplified one-oscillator model (see appendix). However, the qualitative behavior that is dominated by the strongest SiO₂ oscillator remains unchanged. The lower polariton branch starts at the TO frequency and, in the asymptotic limit ($k \rightarrow \infty$), approaches the interface phonon-polariton (IPhP) frequency $\omega_{\text{IPhP}} = 1094 \text{ cm}^{-1}$ of the single interface between silicon and silica which is given by the maximum of $\Im(-1/(\varepsilon_{\text{Lorentz}} + \varepsilon_{\text{Si}}))$.

The two phonon polariton branches represent modes of a qualitatively different polarization [see the insets of Fig. 1(c) schematically displaying the characteristic ionic surface charge distributions]. At ω_{TO} the excitation corresponds to a displacement of ions parallel to the layer, i.e. parallel to the (very large) polariton wavelength, which means a longitudinal polarization [3, 4]. The modes near the LO frequency have a polarization mainly perpendicular to the layer surface which appears as ionic surface charge distribution that has opposite sign on the opposite interfaces. In the short wavelength limit the excitations belonging to the branch near ω_{LO} are mostly localized at the interface of the silica slab with air, whereas the “ ω_{TO} -near branch” is localized at the interface with silicon in the same limit. These high k vector excitations have an almost phononic nature. For decreasing layer thickness the LO (TO) near branch approaches the LO (TO) frequency and both dispersions become more flat due to the increased interaction between the polaritons at the lower and upper interface [3]. The gap between the two polariton branches left also at higher k_{\parallel} is due to the different neighbor media on both sides of the SiO₂ slab. For air (or vacuum) on both sides, the two polarization branches both approach ω_{SPhP} [3, 4].

In usual far-field reflection (transmission) experiments the layer modes are probed by an incident plane wave. However, such plane wave provides only a limited magnitude of wavevector

projection to the plane of the interface and, therefore, is not able to access a notable part of the phonon modes characterized by high k_{\parallel} shown in Fig. 1. On the other hand, modes having k_{\parallel} commensurate with the incident wave can be excited if a suitably polarized plane wave impinges on the substrate. For example, grazing-incidence reflectance of p -polarized light from nanometer-thin layers yields direct information on the energy-loss function which peaks at the LO mode frequency. These spectral features observed as the Berreman effect [15] originate from excitation of low k vector surface phonon-polaritons in the thin film.

In the following we will show that plasmonic antennas are able to change very efficiently the polarization of the electric field in their near-field region and thus excite even phonon-polariton modes that are otherwise dark under plane wave illumination at normal incidence. This allows us to explain the emergence of a strong modification of the plasmon spectrum by a mode that is normally not observed in the far-field spectra without the presence of the plasmonic antenna.

3. Nanoantenna with phononic coating

We study now the influence of a phononic layer that covers the whole gold nanorod on the plasmonic resonance spectrum with use of FDTD simulations (Lumerical FDTD-Solutions v8.7.4). In the simulations, the cylindrical gold antenna is implemented in a large enough simulation cell surrounded by perfectly matched boundary conditions. To account for the small antenna diameter and the thin layer, a mesh size down to 0.75 nm was used around the antenna apex. The antenna was illuminated using a broadband ($800 - 2000 \text{ cm}^{-1}$) plane wave polarized along the long antenna axis. A sufficiently long time evolution was allowed so as to get full convergence of the response. The total-field scattered-field (TFSF) approach was used to separate the computation region into two distinct regions – one containing the total field (sum of the incident field and the scattered field), and the second region containing only the scattered field. The absorption cross section was calculated by summing up the net power flowing inward through a rectangular box enclosing the antenna and the scattering cross section by summing up the power flowing outward through a rectangular box enclosing the TFSF source.

In the FDTD simulations where the gold antenna (characterised by experimental dielectric data [25]) is covered by a phononic layer (described by the previously introduced Lorentz function) with a thickness $t = 30 \text{ nm}$ [see Fig 2(a)], the antenna length has been tuned to match the plasmonic resonance to the maximum of the vibrational energy-loss function. The plasmonic spectra (absorption, scattering, and extinction as sum of the other two) for the covered and bare antenna are shown in Fig. 2(b).

As expected for the bare antenna, a single plasmonic resonance is found, whereas two hybrid modes with frequencies at 1100 cm^{-1} and 1320 cm^{-1} appear in the spectra of the SiO_2 /antenna system. In the spectral region in between these two resonances, the coupled system has become almost transparent due to the influence of the localized dipolar phonon polariton mode of the cylindrical shell. This localized phonon polariton mode is determined by the boundaries imposed by the antenna geometry, and can be understood as a mode emerging from the counterpropagating phonon polaritons at the cylindrical shell characterized by small k vector values ($k \approx n \cdot \pi/l$ with $n = 1$). This means that by covering an antenna featuring strong extinction with a layer characterized by a dark phononic excitation (for normal incidence of light), the antenna becomes transparent if both excitations match spectrally and efficiently couple. This phenomenon, based on the strong coupling between the antenna and the phononic layer resembles the coupling of phonons with bi-layer graphene nanoribbons [26, 27]. In the bi-layer graphene nanoribbons the transparency is reached because the coupling to the graphene's phonons produces a gap in the plasmonic absorption. In our case, however, the gap appears in plasmonic scattering, where a full transparency window is formed, which is not so pronounced in plasmonic absorption, as seen in Fig. 2(b) (red line). Furthermore, the transparency occurs at the position of the phonon-polariton close to the LO frequency [see Fig. 1] and clearly not at the oxide layer's absorption maximum

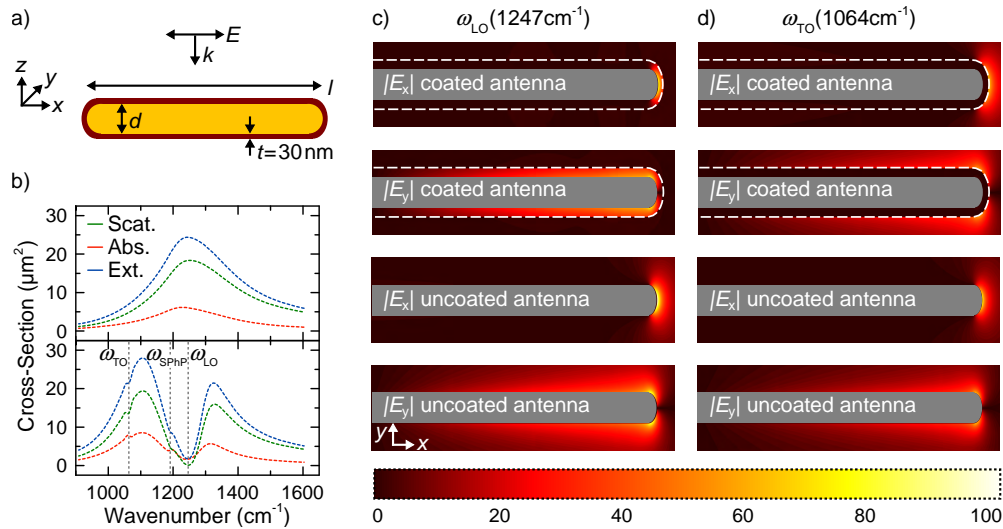


Fig. 2. Gold nanoantenna covered by a phononic layer: (a) Sketch of the investigated gold antenna with length $l = 3200$ nm and diameter $d = 100$ nm coated with a 30 nm thick phononic layer. (b) Simulated far-field resonance spectra (scattering (green), absorption (red), and extinction (blue) cross sections) of a bare gold antenna (upper panel) and an antenna covered with the phononic layer (lower panel). Due to the interaction of the plasmonic excitation and the phononic excitation a transparency window opens in the spectra of the hybrid SiO_2 /antenna system. The corresponding near-field distributions normalized to the electric field amplitude of the incident wave in a cross-section around the antenna at the LO (TO) frequencies are shown in (c) and (d). The antennas's cross section is represented by the grey area.

at the IR-active TO phonon frequency, where only a slight modification of the spectrum is observed. Thus, the excitation of the layer's small k wavevector phonon-polaritons induces the strong coupling with the plasmon-polaritons resulting in a strong modification of the plasmonic scattering.

Figures 2(c) and 2(d) compare the near-field distributions at the LO and TO frequencies with and without the SiO_2 covering shell. These distributions illustrate how the coupled system at resonance becomes transparent due to the coupling with the layer: in the spectral range of the transparency window, the enhanced near-field is almost localized completely inside the layer, at the apex and also along the side walls, as exemplarily shown at the LO frequency. The electromagnetic near-field is thus transferred to the strongly excited short wavevector (long wavelength) surface phonon polariton mode which leads to cloaking of the antenna. In contrast, at the TO frequencies, the electromagnetic fields inside the SiO_2 shell are reduced due to the SiO_2 absorption and because the ionic displacements are almost parallel to the antenna surface. The interaction of the plasmonic excitation with large wavevector (small wavelength) surface phonon polaritons (ω_{SHP}) is similarly weak as could be seen from the small dip at this frequency. This is due to the mismatch of the near-field distribution around the plasmonic antenna and that of the large k wavevector phonon polaritons.

4. Nanoantenna on top of a phononic layer

A configuration which is experimentally easily accessible is shown in Fig. 3(a). Here a gold nanoantenna is placed on top of a phononic layer. In this arrangement, the modes of the planar layer predominantly feature a propagating character compared to the SiO_2 -coated antenna. In the simulations, the plasmonic resonance of the rectangular-shaped gold nanostructures is resonantly

matched to the phononic excitations of a 3 nm thick SiO₂ layer (described with the Lorentz oscillator introduced above) on top of a Si wafer ($n = 3.43$). The antenna-substrate system was illuminated from the substrate direction by a Gaussian beam with perpendicular incidence and polarization along the antenna long axis (scalar approximation: waist radius 4.0 μm , wavenumber range 900 – 2000 cm^{-1}). In order to ensure the accuracy of the calculations, convergence tests were performed. Similar to the shell geometry, at the spectral position of the phonon-polariton a transparency window emerges, which is fully formed only in the scattering spectrum [Fig. 3(b)]. In the absorption and extinction spectra, however, a peak is found in the transparency window at 1191 cm^{-1} . This peak originates from a propagating SPhP which is launched by the scattered light of the antenna.

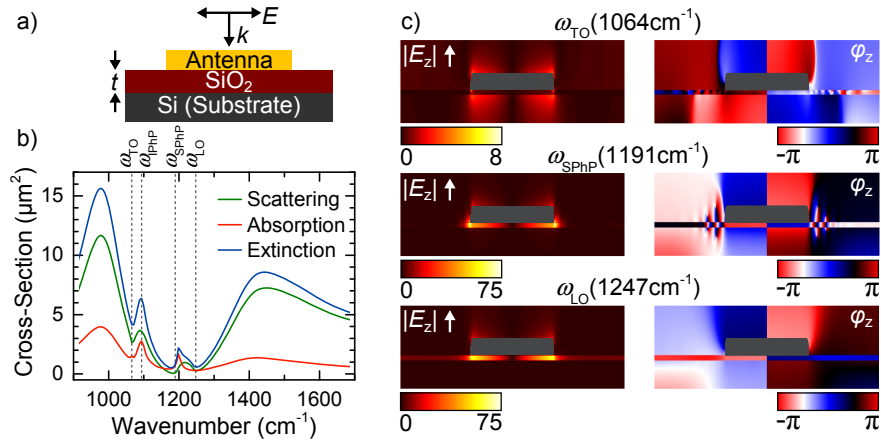


Fig. 3. (a) Schematic drawing of a nanoantenna with length l placed on top of a SiO₂ layer of thickness t . (b) Numerically calculated cross-sections (scattering (green), absorption (red), and extinction (blue)) of a nanoantenna (length $l = 1850$ nm, width and height $w = h = 100$ nm). The SiO₂ layer thickness is 30 nm. (c) Simulated near-field distribution (amplitudes E_z and phase φ_z at the mirror plane) at the wavenumber 1064 cm^{-1} (TO), 1191 cm^{-1} (SPhP) and 1247 cm^{-1} (LO). The area inside the antenna is shown in dark grey.

Looking at the near-field and phase distributions of the hybrid SiO₂/antenna system at different frequencies inside the gap reveals the nature of the phononic modes forming the transparency window. As an example, the phase and near-field distributions at the LO, TO, and SPhP frequencies are shown in Fig. 3(c). A video containing all the frequencies can be found in the supplementary material ([Visualization 1](#)).

At 1191 cm^{-1} (ω_{SPhP}) and 1247 cm^{-1} (ω_{LO}), the z -component of the near-field is almost completely confined inside the dielectric layer. In both cases, the scattered light couples efficiently with the phonon-polariton, which requires also a field component perpendicular to the interface in order to be excited [see Fig. 1(c)]. Considering the phase of the electric field in the z -direction, perpendicular to the antenna, the fields inside the layer and on top of the antenna have a phase difference of π , so that the excitation in the layer quenches that on top of the antenna and thus the coupled system becomes transparent.

Additionally, the phonon-polariton at 1191 cm^{-1} (ω_{SPhP}) propagating along the SiO₂-air interface can be nicely observed in the phase image. For higher frequencies, and therefore smaller wavevectors, as it follows from the dispersion relation shown in Fig. 1(c), the SPhP wavelength increases (see [Visualization 1](#) in supplementary material). In the limit of small wavevectors for the upper polariton branch, corresponding to excitations at the LO frequency, the wavelength becomes infinite leading to a condenser like mode of the SPhP with polarization perpendicular to the layer [see Fig. 1(c)]. Due to the good match of field polarization, the long wavelength

polariton ($\lambda \approx 2 \cdot l$) very efficiently couples to the z -component of the antenna near-field and forms the spectral signature of antenna/SiO₂ hybridization shown in Fig. 3(b).

Looking at Fig. 1(c) again, one could expect a hybridization of the plasmon also with the lower branch of the SPhP similar to the discussed case. This is hampered due to the strong phonon absorption at the TO frequency at which the vibrational polarization is parallel to the layer, see Fig. 3(c) [28, 29]. Only a slight modification indicating the propagating nature of the lower mode is observed in the phase, see [Visualization 1](#).

The complete knowledge on the nature of the hybridized antenna/SiO₂ system is gained by studies on the evolution of the transparency window with different SiO₂ layer thickness and antenna length. For the spectroscopic experiments, nanoantenna arrays were fabricated by means of standard electron beam lithography (EBL) [16, 30] on oxidized silicon wafers with SiO₂ layer thicknesses ranging from $t = 3$ nm to $t = 100$ nm supported by a Si wafer [see Fig. 3(a) and the scanning electron micrograph in the Appendix]. Except the layer thickness of 3 nm caused by natural oxidization, the different silicon dioxide layer thicknesses t were achieved by thermal oxidization. The layer thickness was checked by ellipsometric measurements in the visible spectral range. To improve the adhesion of gold on the SiO₂ an adhesion layer of Ti, with thickness of less than 10% of the gold thickness was used. The mutual antenna distances in the arrays are 10 μm , horizontally and longitudinally, so the antenna-antenna coupling is less important [31, 32]. Each antenna was designed in a cuboid shape with length l , width $w = 60$ nm and height $h = 60$ nm (except for antennas on the natural oxide layer with about 3 nm thickness where $w = h = 100$ nm). The IR measurements of the nanoantenna arrays were performed with a thermal light source using a Bruker Tensor 27 spectrometer coupled to a Bruker Hyperion 1000 IR microscope and a Thermo Fisher NEXUS spectrometer coupled to a NICPLAN microscope, respectively. The measurements were carried out with an aperture leading to beam spot sizes of at least 2500 μm^2 . IR radiation polarized parallel to the long antenna axis was used, since no plasmon can be excited with perpendicular polarized radiation [33]. The transmittance of the SiO₂/antenna system was normalized to a reference taken at an unstructured area on the same sample with same thickness. From the relative transmittance spectra the extinction was calculated and normalized to the geometrical cross-section and the numbers of antennas [16, 30, 32].

Representative spectra of different antenna lengths on top of a 8 nm thick SiO₂ layer are shown in Fig. 4(a). As expected and known from several experimental and theoretical studies, the plasmon resonance shifts with length l according to $\lambda = 2 \cdot n \cdot l \cdot a_1 + a_2$, where n is the refractive index of the surrounding media, a_1 a factor depending on the diameter and material parameters of the antenna and a_2 an offset [34]. For detuned antennas with length $l = 0.9 \mu\text{m}$ the plasmon resonance is located in the mid IR and two distinct peaks appear in the spectrum: the antenna resonance and a peak at 1138 cm^{-1} , which is attributed to the excitation of a surface phonon-polariton at the air-SiO₂ interface [upper branch in Fig. 1(c)]. However, it should be noted that both excitations are already hybridized even though the antennas are strongly detuned. Without any antennas, the SiO₂ vibration of ω_{LO} is dark (under normal incidence of light) and only the momentum k_{\parallel} and the field component E_z provided by the antennas allow for an excitation of the phonon polariton. For longer antennas the resonance shifts towards the SiO₂ vibration and both excitations hybridize strongly. As a consequence, a transparency window between the LO and SPhP frequencies opens, which is strongest for resonantly tuned antennas with $l = 1.5 \mu\text{m}$ and $l = 1.85 \mu\text{m}$. This behaviour is totally consistent with the description introduced earlier.

This behavior is seen more clearly in Fig. 4(b), where the frequencies of the extinction maxima of the hybridized modes are plotted versus the standing wavevector ($k = \pi/l$) of the plasmon polariton of the antenna on top of a 8 nm thick SiO₂ layer [see Appendix for the other layer thicknesses]. As expected, we find a linear dispersion for detuned antennas with this wavevector, far from the point of avoided crossing. In contrast, for an SiO₂ layer without any nanostructures,

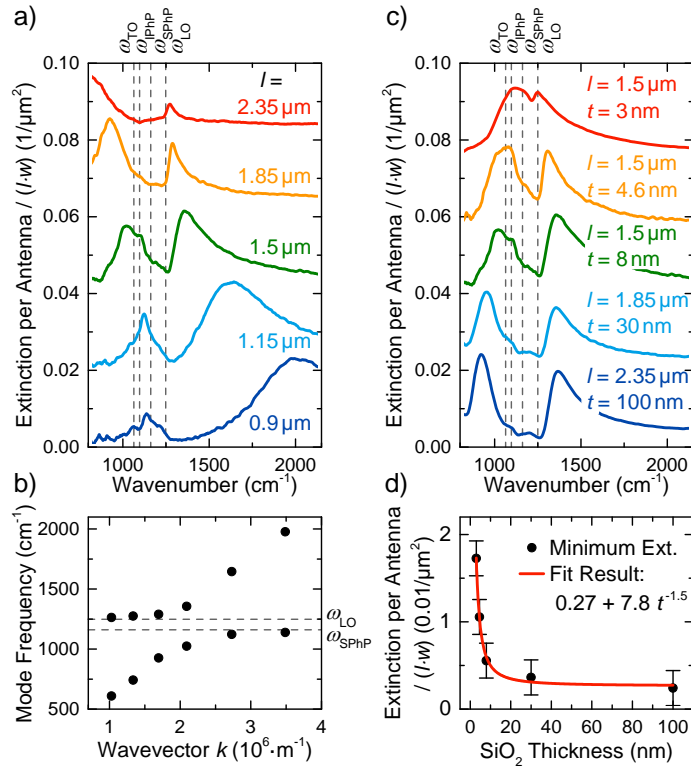


Fig. 4. (a) Extinction spectra (shifted) of nanoantennas (height h and width w are approx. 60 nm) with different length l (see legend) on top of a 8 nm thick SiO₂ layer with a Si wafer beneath. The spectra are derived from relative normal transmittance measured with light polarized parallel to the antenna and the bare SiO₂ layer on Si as reference. A schematic description of the system is shown in Fig. 3(a). Depending on the resonance wavenumber, a transparency window opens between the SPhP and LO frequencies (dashed lines). (b) Resonance positions of hybridized modes taken from (a) versus the wavevector $k = \pi/l$ of the plasmonic excitation. (c) Shifted infrared extinction (parallel polarization) for antennas on SiO₂ with increasing thickness t as given in the figure. The lengths l are resonantly matched to the TO and LO frequencies. (d) Minimum extinction of the spectral dip (transparency window) versus thickness fitted with a power function.

the dispersion of the surface phonon polariton (upper branch) varies only slightly with momentum k_{\parallel} [see Fig. 1(c)]. The slight variation results in different extinction maxima of the hybridized modes: 1247 cm⁻¹ (ω_{LO}) for small momentum (long antennas) and 1138 cm⁻¹ (ω_{SPhP}) for large momentum k_{\parallel} (short antennas) corresponding to the excitation of SPhPs with short and long wavelengths, as discussed previously. For a perfect spectral match, the phonon polariton has a certain frequency between both extrema, which hybridizes with the plasmonic mode and thus forms the transparency window.

In Fig. 4(c) the evolution of the transparency window with SiO₂ layer thickness t is shown. Since the resonance frequency strongly depends on the layer thickness, nanoantennas with resonances tuned to the SiO₂ vibration but different lengths l are selected. The transition from a Fano-type dip (layer thickness of 3 nm and 4.6 nm) to a transparency situation can be clearly observed. Please note that the drop of intensity and the slightly shifted peak minimum between 3 nm and 4.6 nm is not purely caused by the increased layer thickness but also originates from the morphology of the SiO₂ layer resulting in a different permittivity [22]. As described previously,

layers of thicknesses thicker than and equal to 4.6 nm were prepared by thermal annealing whereas the natural oxide layer of 3 nm was used to realize the smallest layer thickness. Obviously, the spectral position of the extinction minimum for small layer thicknesses is located close to the LO frequency corresponding to a dipole moment perpendicular to the interface [see Fig. 1(c)]. For increasing layer thicknesses the transparency extends towards the SPhP frequency due to two reasons. First, the oscillator strength of the SPhP becomes stronger, since more material (more oscillators) is involved. Secondly, the hybridized mode in the high wavevector limit is changed by the non-flat dispersion of the SPhP. As seen in Fig. 1, the slope of the SPhP dispersion increases with layer thickness due to a reduced interaction between the SPhP at the Si-SiO₂ and SiO₂-air interface meaning that for a specific wavevector lower frequencies are found. As a consequence, the hybridized mode in the high wavevector limit approaches ω_{SPhP} for increasing thickness, whereas the hybrid mode in the low wavevector limit remains at the LO frequency.

For oxide layer thickness larger than 30 nm, a full transparency window is formed in the plasmonic extinction. The observation of this strong coupling effect means that the antenna on the SiO₂ layer becomes invisible because it is coupled to the layer that without antenna has a forbidden excitation for normal incidence of light exactly at the plasmonic resonance. These findings are corroborated by the model calculation for the SiO₂-antenna system shown in Fig. 3. Minor differences with respect to the TO absorption and the modulation depth of the transparency window are caused by the assumption of a dielectric function based on a single and very narrow Lorentzian oscillator in the simulations instead of the experimentally determined permittivity (see appendix).

The observed decrease $\propto t^{-1.5}$ of antenna extinction with layer thickness, as shown in Fig. 4(b), consists of two t -dependent factors. These are, on the one hand, the number of oscillators that linearly increases with t and, on the other hand, the near-field enhancement that decreases with the distance from the antenna. Therefore, the total extinction decrease as $\propto t^{-1.5}$, at the phononic resonance means a decay as $\propto t^{-2.5}$ of the near-field intensity into the SiO₂ substrate. Compared to the result of reference [35] where the near-field intensity decay behavior in a weakly IR absorbing organic semiconductor layer was studied, the intensity decay into the SiO₂ is stronger, so that SiO₂ layers thicker than 30 nm do not increase the transparency gap anymore.

5. Summary

Due to strong coupling between phonon-polaritons of thin SiO₂ layers and plasmonic excitations a transparency window is formed in the respective spectra. Although the phonon-polaritons themselves are dark excitations under normal illumination, they strongly interact with plasmon-polaritons as we detailed for a SiO₂ coated linear nanostructure and a planar SiO₂ layer beneath the nanostructures. Among the several phononic surface polariton modes, only the strongest dipolar one, closer to the LO frequency, leads to the transparency window whereas the other phononic modes of large k vector have the effect of slightly modifying the strong coupling. The thickness of the phononic layer is crucial for the dispersion relations of the phonon-polaritons and for their coupling strength to the plasmonic excitation. So, the coupling is Fano-type for very thin-layers and turns into a strong coupling for thicker layers. This coupling is stronger for the surface phonon polariton and almost suppressed for the interface phonon-polariton, the polarization of which is maximum at the interface to the substrate underneath the layer. Because of the coupling to the surface phonon-polariton, the transparency window opens at LO phonon frequency and, with increasing layer thickness, extends over the whole frequency band of the surface phonon-polariton. For the planar system under consideration, a transparency window is present from a layer thickness of only 30 nm on. It is surprising how such thin oxide layers result in strong spectral modification. We suggest the application of the effect in IR devices as sensors and in certain spectral filters.

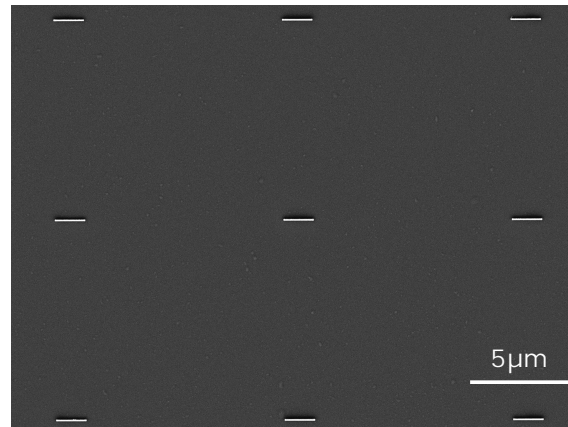


Fig. 5. Scanning electron micrograph of the fabricated and measured gold nanorod arrays on top of a Si wafer with a thermally grown SiO_2 layer of 8.1 nm thickness.

Appendix

Scanning electron micrograph

Experimental data was obtained by measuring relative transmittance spectra of gold nanorod arrays fabricated on Si wafers with thermally oxidized SiO_2 layers. Figure 5 shows a scanning electron micrograph of an antenna array with length $l = 1.5 \mu\text{m}$ and SiO_2 layers thickness of 8.1 nm.

Mode hybridization for different SiO_2 layer thicknesses

For comparison to Fig. 4(b), Fig. 6 shows the frequencies of the extinction maxima of the hybridized modes plotted versus the standing wavevector ($k = \pi/l$) of the plasmon polariton of the antenna for all layer thicknesses. A linear dispersion for detuned antennas with this wavevector, far from the point of avoided crossing, is found for all layer thicknesses. For the thinnest SiO_2 layer an avoided crossing at the LO frequency is observed. With increasing layer thickness the splitting is larger due to increased coupling of the antenna and the small k wavevector phonon polariton modes. The splitting extends down to the TO frequency for the 100 nm thick layer [see the dashed lines in Fig. 6].

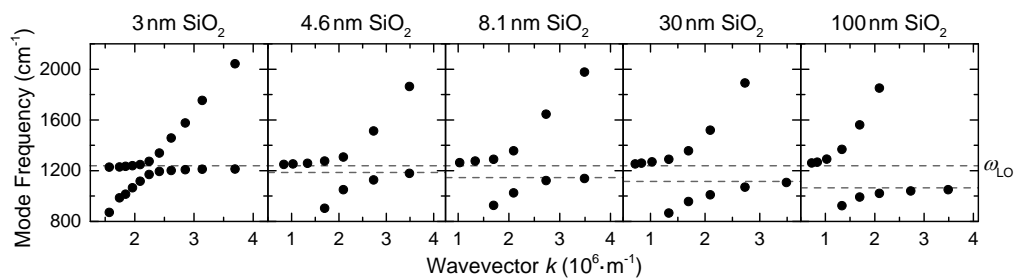


Fig. 6. Resonance positions of measured hybridized modes for different SiO_2 layer thicknesses versus the wavevector $k = \pi/l$ of the plasmonic excitation. For the thinnest SiO_2 layer an avoided crossing at the LO frequency (upper dashed grey line) is observed. For increasing layer thickness (increasing coupling strength) the splitting extends to the TO frequency, as indicated by the lower horizontal dashed lines.

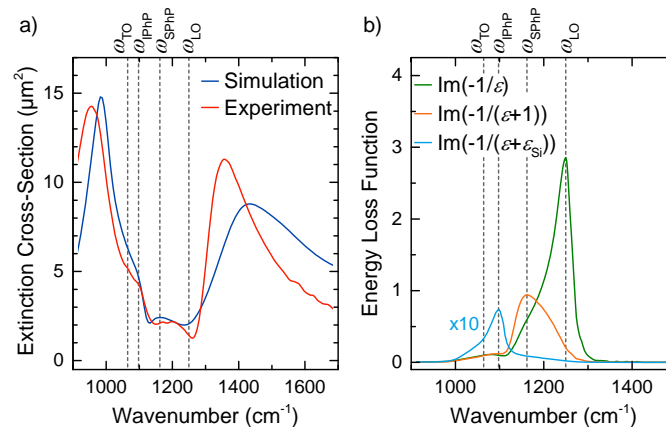


Fig. 7. (a) Simulated extinction cross-section (blue) of plasmonic antennas ($l = 1.85 \mu\text{m}$) on top of a 30 nm thick SiO_2 layer simulated with the dielectric function experimentally determined by Gunde et al. [23] compared to the measurement shown in red. (b) Energy loss functions derived from the dielectric function used for the simulations shown in (a).

Differences between experimental results and calculated spectra

The minor differences between experimental results and calculated spectra can be explained by different optical properties of the layer. In Fig. 7(a) a plasmonic antenna ($l = 1.85 \mu\text{m}$) on top of a 30 nm thick SiO_2 layer is simulated with experimental dielectric data measured by Gunde [23] and compared to the measured spectrum. Analogous to Fig. 1(a) (bottom panel), Fig. 7(b) is showing the energy loss functions following from the Gunde data. The results make obvious the effects from damping and other oscillators in the real SiO_2 and show that the dielectric function of Gunde can describe the measured data much better compared to the Lorentzian dielectric function.

Funding

J.V. and C.H. acknowledge financial support by the Heidelberg Graduate School of Fundamental Physics. C.H. acknowledges financial support by the Helmholtz Graduate School for Hadron and Ion Research. This research was supported in part by the bwHPC initiative and the bwHPC-C5 project provided through associated compute services of the bwForCluster MLS&WISO (Production) at Heidelberg University and the University of Mannheim. J.A. and T.N. acknowledge the project FIS2013-14481-P from the Spanish Ministry of Economy and Competitiveness (MINECO) from the Department of Education of the Basque Government, IT756-13 of consolidated groups, and ETORTEK project nanoGUNE'14 from the Department of Industry of the Basque Country Government. F.N. acknowledges financial support by the Baden-Württemberg-Stiftung (PROTEINSENS). T.Nagao is supported from CREST, Japan Science and Technology Agency (JST) and from KAKENHI, Japan Society for the Promotion of Science (JSPS).

Acknowledgments

We acknowledge SOLEIL for provision of synchrotron radiation facilities, and we would like to thank P. Dumas and F. Jamme for assistance in using the spectrometers at the beamline SMIS. F.N. thanks M. Hentschel for fruitful discussions. T.Nagao acknowledges A. Ohi and T. Ohki for the fabrication of Au antennas. We acknowledge the financial support of the DFG and Heidelberg University within the funding program Open Access Publishing.